Journal of Molecular Catalysis A: Chemical 297 (2009) 26–34

Contents lists available at ScienceDirect

Journal of Molecular Catalysis A: Chemical

journal homepage: www.elsevier.com/locate/molcata

Effect of preparation method on structural characteristics and propane steam reforming performance of Ni–Al_2O_3 catalysts

Lingzhi Zhang, Xueqin Wang, Bing Tan, Umit S. Ozkan*

Department of Chemical and Biomolecular Engineering, The Ohio State University, 140 West 19th Avenue, Columbus, OH 43210, United States

ARTICLE INFO

Article history:
Received 6 May 2008
Received in revised form 5 September 2008
Accepted 10 September 2008
Available online 18 September 2008

Keywords:
Nickel catalyst
Sol–gel preparation
Metal–support interaction
Steam reforming
Deactivation
Sintering
Coking
Carbon filament

ABSTRACT

Propane steam reforming was studied over Ni–Al_2O_3 catalysts that were prepared by a conventional impregnation (IM) method and a one-step sol–gel (SG) technique. Both Ni–Al_2O_3 catalysts showed similar initial activity. However, IM-Ni–Al_2O_3 deactivated severely with time-on-stream of propane steam reforming. The catalyst prepared using a SG technique demonstrated stable catalytic performance. The two catalysts also showed major differences in product distribution, with SG catalyst giving much higher yields of hydrogen. Catalysts were characterized with temperature-programmed reduction (TPR), X-ray photoelectron spectroscopy (XPS), temperature-programmed oxidation (TPO), transmission electron microscopy (TEM), X-ray diffraction (XRD) and Raman spectroscopy. It was revealed that, with sol–gel preparation, highly dispersed small Ni crystallites are formed with a strong interaction with the support. This is shown to be important for coke suppression and catalyst stability.

1. Introduction

Steam reforming of hydrocarbons has seen increasing interest due to the necessity of efficient and cost-effective reforming technologies for hydrogen production for fuel cell applications. In practice, steam reforming of hydrocarbons, especially that of methane, is performed at high temperatures over Ni-based catalysts where the lower cost of nickel is an important advantage. Current Ni-based catalysts, which are used for natural gas steam reforming processes, suffer from catalyst deactivation by coke formation and sintering of metallic Ni active phase [1–3]. It is generally agreed that coke deposition is the major cause for activity loss. Boudouard reaction ($2CO \rightarrow C + CO_2$) and methane/hydrocarbon decomposition [4] are two major side reactions during hydrocarbon steam reforming, which could lead to filamentous carbon accumulation at the surface of Ni catalysts [5]. The coking process expedites active metal degradation and activity loss. Carbon growth is significantly decelerated on noble metals because carbon could not dissolve in them [2,6,7]. Therefore, supported precious metals such as Pd, Pt, and Rh are adopted for hydrocarbon reforming reactions and have exhibited superior activity and stability [8–13]. However, the cost of the precious metals is still a major drawback. The low-cost and long-proven performance of Ni-based catalysts, therefore, still warrant the effort to optimize these catalysts for steam reforming applications, particularly for fuel processing from existing liquid fuels such as gasoline and diesel.

Extensive efforts have been made on development of Ni catalysts with improved resistance to coke formation. The support material has been found to exert a strong influence on the reactivity of CH_x surface intermediates formed during hydrocarbon reforming [7,14]. The number of hydrogen atoms in surface CH_x species is relevant to the coking resistance of Ni catalysts [15]. Lower x values tend to result in the formation of carbonaceous deposits, a precursor of surface coke deposition. The nature of the support materials has been investigated in recent years in an attempt to seek supports with the desired acid–base or redox properties for the catalysts or modify existing supports by addition of promoters to enhance the reactivity of surface intermediates or suppress coke dissolution [16]. Alkali metal oxides such as K_2O and CaO have been shown to improve coking resistance by enhancing carbon gasification, but at the expense of catalytic activity [1,17]. The introduction of a small amount of molybdenum or tungsten (0.5 wt% MoO_3 or WO_3) into Ni catalysts has been shown to increase the coking resistance without loss in catalytic activity [18–22]. Alternatively, lanthanides emerge to be promising promoters because they can inhibit coke formation without sacrificing the catalytic activity [23–25]. Zhuang et al. [23] investigated the effect of cerium oxide as the promoter in $MgAl_2O_4$-supported Ni catalysts for methane steam reforming at

* Corresponding author. Tel.: +1 614 292 6623; fax: +1 614 292 3769.
E-mail address: ozkan.1@osu.edu (U.S. Ozkan).

1381-1169/$ – see front matter © 2008 Elsevier B.V. All rights reserved.
doi:10.1016/j.molcata.2008.09.011

550 °C. Cerium promotion showed a beneficial effect by not only decreasing the rate of carbon deposition, but also increasing the catalytic activity. Wang and Lu [24] stated that the addition of CeO_2 into Ni/Al_2O_3 catalysts enhanced the nickel dispersion and reactivity of carbon deposits, leading to an improvement in the catalytic activity and stability in CO_2 reforming of methane. Earlier work from our group has shown that incorporation of lanthanides into the Ni matrix reduces coking by inhibiting the diffusion of carbon into Ni particles [26,27].

Metal–support interaction is another phenomenon that affects carbon deposition in steam reforming. The metal–support interaction was found to correlate with Ni particle size, Ni dispersion and morphology [28]. It has been discussed in literature [29–31] that smaller Ni particle size and higher dispersion can minimize Ni sintering at high temperatures or long-term operation and improve coking resistance, therefore enhancing catalyst stability during hydrocarbon reforming. The propensity to coking, to a large extent, depends on the size of Ni particles. It is reported by Edwards and Maitra [14] that it requires an ensemble of 6 or 7 atoms of Ni to catalyze carbon formation and growth whereas only 3 or 4 atoms of Ni are needed for the CH_4 reforming reaction. Stronger metal–support interaction has been proven to enhance Ni dispersion dramatically, which would prevent the formation of large Ni clusters not only during catalyst preparation and activation, but also in the high temperature reaction process. It was reported in Liu et al.'s work [32] that nickel oxides interacting weakly with the support tend to aggregate and sinter during catalyst reduction and reforming and lead to activity loss. Similarly in Wang et al.'s studies [33], suppression of coke formation and Ni sintering were attributed to solid solution formation between active metals and the support. However, on the other side, the interaction between Ni and the support leads to the formation of solid solution or other mixed oxide compounds and sharply decreases the amount of available Ni for the targeted steam reforming reaction. This can be compensated by increasing the doping amount of Ni. Magnesia has been found capable of controlling the size of metallic clusters for $Ni–Al_2O_3$ system [14]. The presence of mobile Ti–O in Ni/TiO_2 could break the large ensembles of Ni atoms, which stimulate coke formation [7]. Other promoters including B, Ge, Ga and Zn were also examined for modifying metal–support interactions [34].

In addition to doping other elements to enhance the interaction, another strategy is development of novel preparation techniques to improve metal dispersion and coking resistance. Co-precipitation method was adopted in Pelletier et al.'s work [16] and it is evidenced that this method is effective in achieving high dispersion and improving coking resistance. Creation of solid solutions between NiO and MgO during catalyst synthesis yields crystals of smaller size with high reaction activity and stability [32,33,35].

In this study, structural characteristics and propane steam reforming performance of $Ni–Al_2O_3$ catalyst prepared by a sol–gel technique were examined and compared to those of $Ni–Al_2O_3$ catalyst prepared by a conventional impregnation. Although the low temperatures chosen for the propane reforming can classify the reaction as "pre-reforming", the term "steam reforming" is used in view of the significant levels of hydrogen yields obtained. Characterization was performed using the BET method with N_2 adsorption, H_2 chemisorption, X-ray photoelectron spectroscopy, temperature-programmed reduction, temperature-programmed oxidation, X-ray diffraction, Raman spectroscopy and transmission electron microscopy. It was found that, with the SG technique, Ni species interact strongly with the Al_2O_3 support, which could resist sintering of Ni species and retard the formation of carbon fibers. This study is a continuation of the work where the effect of lanthanide promotion on catalytic performance and deactivation characteristics of lanthanide-promoted $Ni–Al_2O_3$ catalysts in propane steam reforming were examined [26,27].

2. Experimental

2.1. Catalyst preparation

$Ni–Al_2O_3$ catalysts were prepared using a SG technique and a conventional IM method. Nickel precursor (Aldrich) used during catalyst preparation was in nitrate form. Aluminum tri-*sec*-butoxide (ATB; Aldrich) was used as aluminum precursor. For SG synthesis, ethanol (Alfa Aesar) was used as the solvent. The following variables were controlled during the synthesis: nickel content = 20 wt%, H_2O/ATB molar ratio = 3.6, and pH of the resulting gels = 4.8. Initially, ATB was dissolved in ethanol. The aqueous solution with the desired amount of nickel was added drop-wise into the ethanol solution using a syringe pump at a flow rate of 0.5 cm^3/min. The pH of the resulting green gels was measured and adjusted by adding HNO_3 (Fisher) or NH_4OH (Fisher). The gels were stirred for an additional 15 min and were kept at room temperature for 30 min. The samples were then dried overnight in the oven at 110 °C to remove the remaining water and ethanol. The dry samples were ground to fine powders and were calcined under O_2 at 450 °C for 4 h. For the IM synthesis, the Al_2O_3 support was prepared first with the SG technique as described above. Ni species were introduced onto the Al_2O_3 support using impregnation in aqueous solution. The IM catalysts were then dried and calcined under the same conditions as for the SG catalysts.

2.2. Characterization

2.2.1. BET surface area and H_2 chemisorption

The surface areas of oxidic samples calcined at 450 °C in O_2 were measured using the BET method with a Micromeritics ASAP 2010 instrument, using N_2 as the adsorbent at liquid N_2 temperature (77 K). Samples were degassed at 130 °C for 12 h under vacuum before surface area measurements. The volumetric measurement of H_2 chemisorption was conducted using a Micromeritics ASAP 2010 Chemisorption system. Prior to adsorption measurements, calcined samples were reduced *in situ* under H_2 at the desired reduction temperature (600 °C) for 2 h followed by evacuation to 10^{-5} mmHg and cooling down to 35 °C. Adsorption isotherms were measured at equilibrium pressures between 50 mmHg and 500 mmHg. The first adsorption isotherm was established by measuring the amount of gas adsorbed as a function of pressure. After completing the first adsorption isotherm, the system was evacuated for 1 h at 10^{-5} mmHg. Then a second adsorption isotherm was obtained. The amount of probe molecule chemisorbed was calculated by taking the difference between the two isothermal adsorption amounts.

2.2.2. TPR studies

Temperature-programmed reduction of catalysts was conducted using a laboratory-made gas flow system described in detail elsewhere [36]. 50 mg sample was loaded in a 1/4 in. O.D. quartz U-tube reactor. The sample was then heated under 10% O_2/He at 450 °C for 1 h followed by cooling to room temperature under Ar. The reduction was performed with 10% H_2/Ar (40 cm^3 (STP)/min). The reactor temperature was raised using a ramp rate of 10 °C/min to 900 °C and held at that level for 10 min. To remove moisture formed during reduction, effluents from the reactor were sent through a silica gel water trap before reaching the detector. H_2 consumption was measured continuously as a function of sample temperature using a thermal conductivity detector (TCD) connected to a data-acquisition system.

2.2.3. XRD studies

In situ X-ray diffraction patterns during reduction of catalysts were obtained with a Bruker D8 Advance X-Ray diffractometer equipped with an atmosphere and temperature control stage and using Cu Kα radiation (λ = 1.542 Å) operated at 40 kV and 50 mA. The powder diffraction patterns were recorded in the 2θ range from 20° to 80°. Reduction was performed *in situ* under 5% H_2/N_2 gas flow using a linear temperature-program between isothermal steps (50 °C). The catalysts were kept at isothermal steps for 0.5 h before data collection and the ramp rate between the consecutive isothermal steps was 10 °C/min.

2.2.4. XPS studies

X-ray photoelectron spectroscopy analysis was performed using an AXIS Ultra XPS spectrometer, operated at 13 kV and 10 mA with monochromator Al Kα radiation (1486.6 eV). Samples were reduced with 20% H_2/N_2 at 600 °C for 2 h in a reactor. The reduced samples were then sealed using the valves located at both ends of the reactor. The reactors were then taken to an argon–atmosphere glove box, where the catalysts were removed out of the reactors and mounted on the XPS sample holders using a conductive carbon tape. The sample holders were transferred to the XPS chamber without exposing them to the atmosphere using a controlled-atmosphere transporter. All spectra were corrected using the C 1 s signal located at 284.5 eV.

2.2.5. TPO studies

Temperature-programmed oxidation of post-reaction catalysts was performed using a laboratory-made gas flow system. Initially, 10 mg of post-reaction catalyst was placed in a 1/4 in. O.D. quartz U-tube reactor and was heated under He (40 cm^3 (STP)/min) at 400 °C for 30 min to remove adsorbed moisture and other species (e.g. CO_2). During TPO, the reactor temperature was raised under 5% O_2/He (40 cm^3 (STP)/min) with a ramp rate of 10 °C/min to 900 °C. Effluents from the reactor were continuously monitored as a function of sample temperature using a mass spectrometer (Thermo Finnigan Trace GC ultra-Trace DSQ MS) with He as the carrier gas.

2.2.6. Raman studies

Raman spectroscopy was conducted with a Horiba Jobin-Yvon LabRam HR800 spectrometer. The illumination source employed is an internal HeNe laser with 633 nm wave length. The instrument is equipped with a CCD detector and a standard Olympus microscope. The laser power at the sample was controlled below 3 mW to avoid laser heating effects. Post-reaction samples used for TPO and Raman analysis were kept on-line using a feed stream of $C_3H_8/H_2O/N_2$ = 1/4/95 at 500 °C for 28 h.

2.2.7. TEM studies

TEM images were collected from Tecnai TF-20 operated at 200 kV. Post-reaction samples were ultrasonically dispersed in ethanol. A drop of the suspension was then deposited on a Cu grid for TEM observation.

2.3. Reaction studies

Propane steam reforming reaction experiments were performed using a stainless steel fixed-bed flow reactor (1/4 in. O.D.). Catalytic performance of different catalysts were compared using an equal surface area loading (5 m^2) in the reactor at 500 °C and $C_3H_8/H_2O/N_2$ = 1/4/80 with a total flow rate at 170 cm^3/min. Prior to a reaction, the catalyst was reduced *in situ* under 20% H_2/N_2 at 600 °C for 2 h. Effluents from the reactor were analyzed using an automated Shimadzu GC-14A equipped with flame ionization detector (FID) and TCD detectors. Separations were performed under Ar using two columns: Porapak Q (12 ft × 1/8 in. SS, 80/100 mesh) and Molecular Sieve 13× (5 ft × 1/8 in. SS, 60/80 mesh). A GOW-MAC 069-50 ruthenium methanizer operated at 350 °C was used with the FID for accurate quantification of CO down to 10 ppm concentration level. The post-reaction samples were passivated with 1% O_2 in He for 2 h at room temperature before being unloaded. Then they were saved in a desiccator for TEM experiments.

Below are definitions used for catalytic performance calculations.

$$\%C_3H_8 \text{ conversion} = \frac{\text{moles of propane converted}}{\text{total moles of propane in the feed}} \times 100$$

$$\%H_2 \text{ yield} = \frac{2 \times \text{moles of } H_2 \text{ produced}}{\text{total moles of hydrogen in the feed}} \times 100$$

$$\%\text{C-containing product selectivity for A} = \frac{\text{moles of C in product A}}{\text{moles of C in all C-containing products}} \times 100$$

3. Results and discussion

3.1. Physical surface area and metallic Ni surface area

Table 1 lists the physical surface area of calcined catalysts and the bare support and the metallic Ni surface area of reduced catalysts. IM-Ni–Al_2O_3 catalyst was prepared by impregnating $Ni(NO_3)_2$ onto a sol–gel prepared Al_2O_3 support. SG-Ni–Al_2O_3 catalyst was prepared by a sol–gel technique with precursors of $Ni(NO_3)_2$ and aluminum tri-*sec*-butoxide in an ethanol solvent. IM-Ni–Al_2O_3 catalyst has a lower surface area compared with SG-Ni–Al_2O_3 catalyst, which is possibly due to loss of pore size caused by Ni impregnation [16]. This is supported by the pore volume measurement that IM-Ni–Al_2O_3 has a pore volume of 0.26 cm^3/g in comparison with 0.63 cm^3/g for SG-Ni–Al_2O_3.

H_2 uptakes at mono-layer coverage of the metallic Ni were used to estimate surface Ni atom area for reduced catalysts, assuming that each surface Ni atom chemisorbs one hydrogen atom ($H/Ni_{surface}$ = 1). It should be noted that H_2 chemisorption is a measurement of reducible Ni species on the surface. Reduced SG-Ni–Al_2O_3 catalysts demonstrate a lower metallic surface area than reduced IM-Ni–Al_2O_3 catalysts. This can be possibly attributed to two reasons. First, the impregnation method may lead to more Ni species staying on the surface instead of entering the bulk as in sol–gel preparation. Another reason is that for Ni species exposed on the surface in both catalytic systems, variation in extents of reduction may exist. In IM catalysts, large Ni particles of weak interaction with neighbouring support could make these Ni species easy to reduce. However, in SG catalysts, as would be evidenced by XPS or XRD results in later sections, there are much smaller Ni crystallites and stronger interaction between Ni and the

Table 1
Surface area and metallic Ni surface area.

Sample	Surface area (m^2/g)	Metallic Ni surface area (m^2/g)
SG-Al_2O_3	300	
O-450-20% IM-Ni–Al_2O_3	204	
O-450-20% SG-Ni–Al_2O_3	238	
R-600-20% IM-Ni–Al_2O_3		9.4
R-600-20% SG-Ni–Al_2O_3		6.8

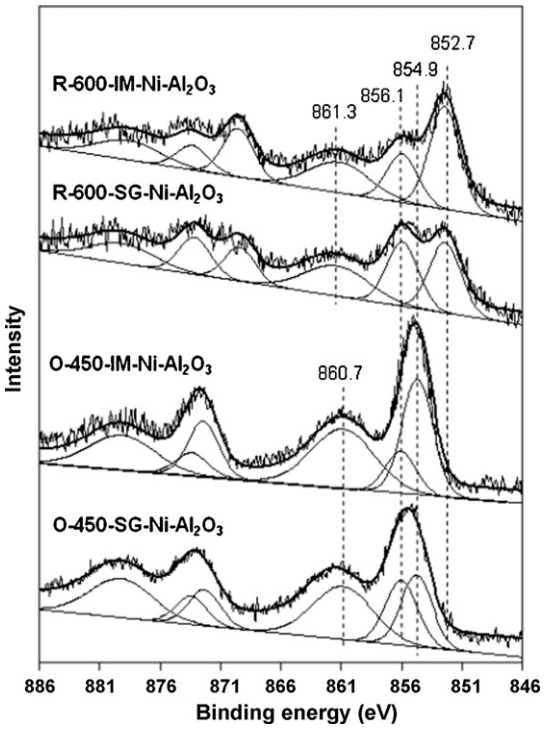

Fig. 1. X-ray photoelectron spectra (Ni 2p region) of Ni–Al_2O_3 catalysts. O-450: calcined at 450 °C; R-600: reduced at 600 °C.

support. Therefore, complete reduction of Ni species on the surface is difficult for the reduction conditions employed during H_2 chemisorption.

3.2. XPS of Ni species in calcined and reduced catalysts

Fig. 1 presents the Ni 2p region of the X-ray photoelectron spectra of Ni–Al_2O_3 catalysts calcined at 450 °C and reduced at 600 °C (O-450 and R-600). For peak identification, the spectra were deconvoluted based on the constraints of equal spin-orbit splitting for Ni 2p peaks, the height ratio of Ni $2p_{3/2}$ to Ni $2p_{1/2}$ being constant at 2 (theoretical value), and the full width at half maximum (FWHM) of these peaks being equal. For calcined catalysts, the peak located between 855 eV and 857 eV can be interpreted as a combination of two Ni $2p_{3/2}$ peaks with binding energies of 854.9 eV and 856.1 eV. There have been previous investigations of the XPS Ni 2p spectral region in the Ni–Mo–γ-Al_2O_3 system by our group [37] as well as by others [38,39]. The peak at 854.9 eV suggests the presence of NiO on the surface, which can be supported by strong shake-up lines around 860.7 eV ($2p_{3/2}$), indicative of Ni^{2+} species. There has been no affirmative assignment of the peak at 856.1 eV reported in the literature, with the possibility of $NiAl_2O_4$ or Ni_2O_3. We tend to ascribe this feature to a spinel $NiAl_2O_4$ structure on the surface, which can be supported by our preparation methods creating a stronger bonding between Ni and the Al_2O_3 support. This assignment is also in agreement with findings obtained from other characterization results presented in the paper. The "surface spinel" model proposed by Jacono et al. [38] where Ni^{2+} ions occupy the tetrahedral sites in γ-Al_2O_3 again supports this possibility. The two deconvoluted peaks described earlier (NiO–854.9 eV and $NiAl_2O_4$–856.1 eV) were integrated and the quantified percentages were shown in Table 2. SG-Ni–Al_2O_3 exhibits a larger portion of $NiAl_2O_4$ species, 49% in comparison to 27% for that of IM-Ni–Al_2O_3. Impregnation catalysts have more NiO species on the surface.

Table 2
Content of Ni species for catalysts prepared by impregnation and sol–gel methods: calcined and reduced samples.

Sample	Ni species (%)		
	Ni-852.7	Ni-854.9	Ni-856.1
O-450-IM-Ni–Al_2O_3	–	73	27
O-450-SG-Ni–Al_2O_3	–	51	49
R-600-IM-Ni–Al_2O_3	70	–	30
R-600-SG-Ni–Al_2O_3	53	–	47

After a reduction step at 600 °C, the NiO peak at 854.9 eV disappeared, replaced by a new peak centered at 852.7 eV ($2p_{3/2}$). This corresponds to metallic Ni species as a result of NiO reduction. It was noted that, over both catalysts, NiO species were completely converted to metallic Ni species under our reduction conditions. However, there were negligible changes for the peak at 856.1 eV. One can conclude that NiO on the support surface can be reduced more easily whereas the Ni species at Ni $2p_{3/2}$ of 856.1 eV is hardly reduced at 600 °C, which is most likely $NiAl_2O_4$ species instead of Ni_2O_3 mentioned earlier. Studies from literature [37,39] reveal that $NiAl_2O_4$ species is much more difficult to be reduced compared to NiO species.

From the Ni 2p region of reduced catalysts (Fig. 1 and Table 2), for IM-Ni–Al_2O_3, a larger portion of metallic Ni (70% compared with 53% for that of SG-Ni–Al_2O_3) was detected on the surface, which explains the H_2 chemisorption measurement that there are more reducible Ni species on the impregnated catalyst surface and the sol–gel catalyst has a substantially lower degree of reduction due to spinel formation.

3.3. X-ray diffraction

In situ X-ray diffraction patterns were collected during a step-wise temperature-programmed reduction process where a calcined sample was reduced in 5% H_2/N_2 (Fig. 2). 5% H_2/N_2 was chosen instead of 20% H_2/N_2 used in reaction testing because of safety regulations imposed by the facility. Diffraction patterns were collected at different temperatures including 450 °C, 500 °C, 600 °C, 700 °C and 800 °C. At each temperature, a 30 min holding time was used before data collection. The International Center for Diffraction Data (ICDD) library was used for phase identification. The major diffraction features observed over the oxidized samples (R-27 °C) are characteristic of γ-Al_2O_3 and correspond to (3 1 1), (4 0 0) and (4 4 0) diffraction lines. Other possible crystalline phases present in the calcined catalysts could be bulk NiO or $NiAl_2O_4$ because they have overlapping diffraction lines with γ-Al_2O_3 phase. With an increase in reduction temperature, the (4 4 0) diffraction line shifts to a higher angle. The diffraction lines from metallic Ni appeared after reduction above 450 °C for both Ni–Al_2O_3 catalysts prepared by the IM method and SG technique. The intensity of metallic Ni diffraction lines from Ni–Al_2O_3-IM catalyst grows faster than those from Ni–Al_2O_3-SG catalyst. Meanwhile the diffraction lines become sharper with increasing reduction temperatures. These results indicate that the Ni species in impregnation catalysts can be reduced more easily and form larger metallic particles. Because of the overlap between Al_2O_3 (4 0 0) diffraction line and the most intensive metallic Ni (1 1 1) diffraction line, Ni (2 0 0) diffraction line broadening was used to calculate the metallic Ni crystallite size with Scherrer equation. The FWHM was obtained with GRAM software. The calculated results are reported in Table 3. For both Ni–Al_2O_3 catalysts, they started with the same Ni crystallite size at 500 °C (9 nm). With increase in reduction temperature, the crystallite Ni size tends to grow larger, evidenced

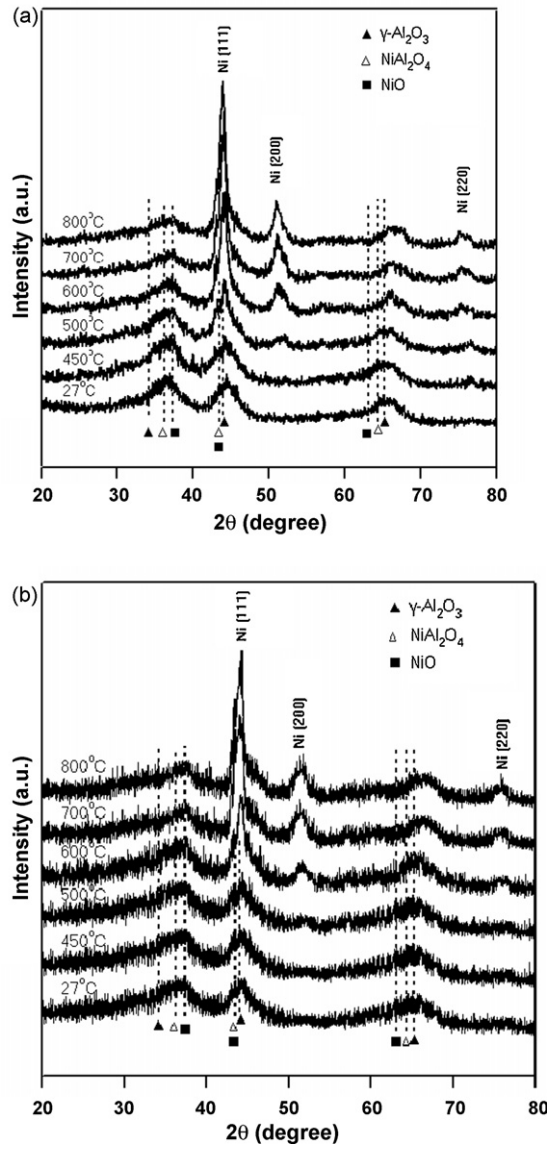

Fig. 2. *In situ* X-ray diffraction patterns of Ni–Al_2O_3 catalysts prepared by (a) impregnation method and (b) sol–gel technique during temperature-programmed reduction.

by sharper and more intense diffraction lines. For sol–gel catalysts, metallic Ni size stabilized at 13 nm whereas for impregnated catalysts, it continued to grow with increase in reduction temperatures. By 800 °C, this size was more than double the size at 500 °C. These findings are consistent with other characteristics of the sol–gel preparation technique (high BET surface area, improved thermal stability, small particle size) summarized by Gonzalez et al. [40]. The weaker metal–support interaction in impregnated catalysts makes the Ni particles aggregate more easily into polymeric structures and form bigger Ni particles after reduction.

Table 3
Ni crystallite size after reduction at different temperatures.

Catalyst	*d* (nm) at different reduction temperatures (°C)			
	500	600	700	800
IM-Ni–Al_2O_3	9	15	17	20
SG-Ni–Al_2O_3	9	12	13	13

Note: Calculation based on broadening of Ni (2 0 0) diffraction lines.

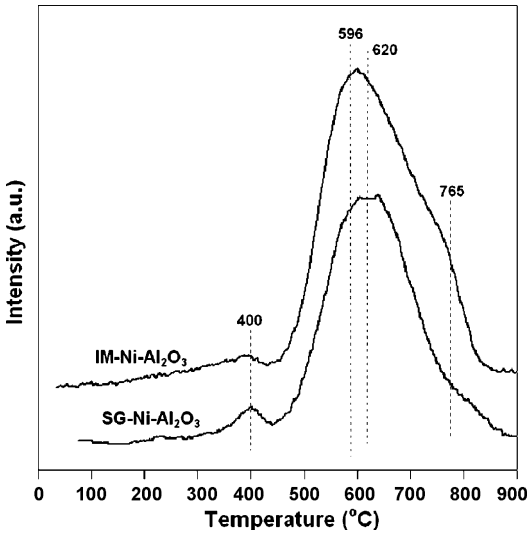

Fig. 3. Temperature-programmed reduction profiles of Ni–Al_2O_3 catalysts.

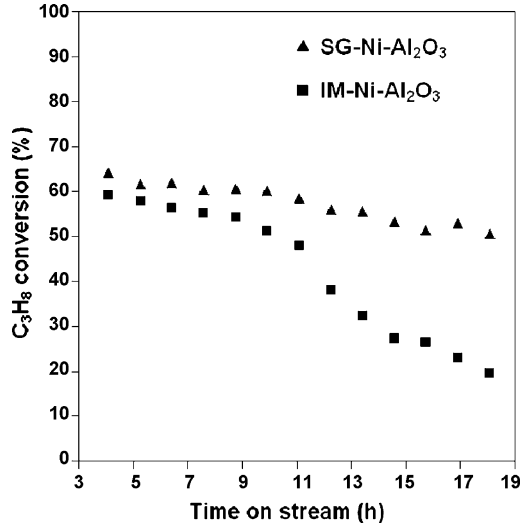

Fig. 4. Time-on-stream performance of Ni–Al_2O_3 catalysts during steam reforming reaction: %propane conversion.

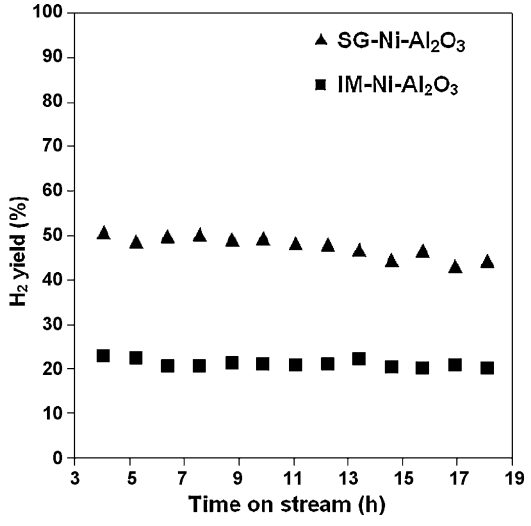

Fig. 5. Comparison of H_2 yields over Ni–Al_2O_3 catalysts during propane steam reforming.

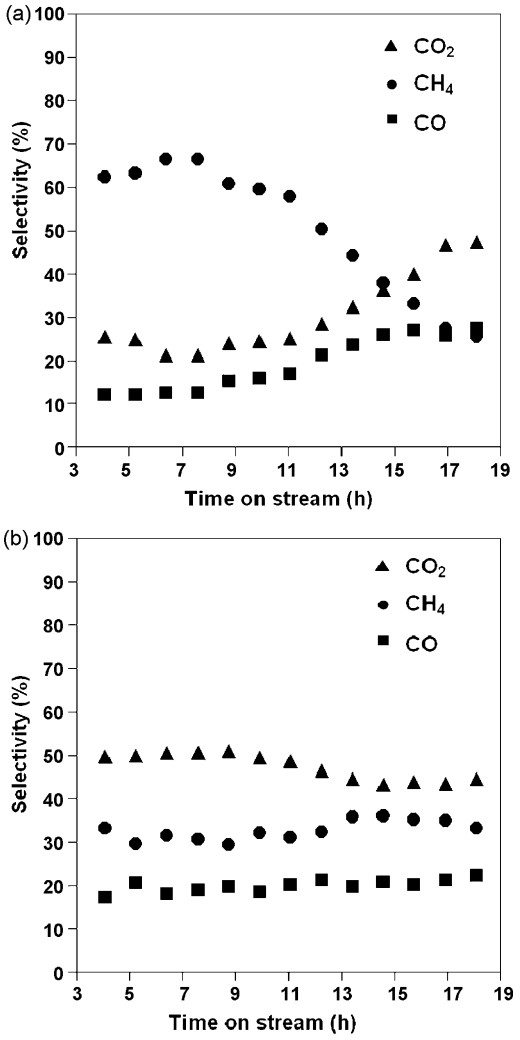

Fig. 6. C-containing product distribution during steam reforming reaction of propane: (a) IM-Ni–Al_2O_3 catalyst; (b) SG-Ni–Al_2O_3 catalyst.

3.4. TPR profiles of Ni–Al_2O_3 catalysts

Temperature-programmed reduction experiments on Ni–Al_2O_3 catalysts were performed using 10% H_2/Ar as the reducing agent. As shown in Fig. 3, TPR profiles exhibit two distinct reduction features accompanied by a shoulder peak at high temperature. A small low temperature reduction peak around 400 °C could be assigned to the reduction of trace amounts of NiO clusters or bulk NiO weakly interacting with the support, which was reported in Song et al.'s work [41] as the approximate reduction temperature for unsupported NiO. Also in their publication, Ni species supported on γ-Al_2O_3 show a reduction feature at 500–700 °C. Correspondingly in our TPR profiles, the broad high temperature reduction peak around 600 °C can be ascribed to the reduction of NiO_x species that have stronger binding to the support. Sol–gel catalyst displays a slight shift of this reduction peak (at 620 °C) compared with impregnated catalyst (at 596 °C). Further interaction between NiO and the support would lead to the formation of $NiAl_2O_4$, which could not be reduced until 800 °C [41]. The tail reduction peak after 800 °C for SG-Ni–Al_2O_3 might have contributions from $NiAl_2O_4$ reduction. The H_2 consumption can be determined by integrating the peak area under the TPR curve for the two Ni–Al_2O_3 catalysts. An area ratio of 1.3 was obtained for IM-Ni–Al_2O_3 over SG-Ni–Al_2O_3. This suggests that more Ni species can be reduced over impregnated catalysts, which is consistent with our statement that there is stronger metal–support interaction for sol–gel catalysts and this structure difference yields more reducible NiO species for impregnated catalysts.

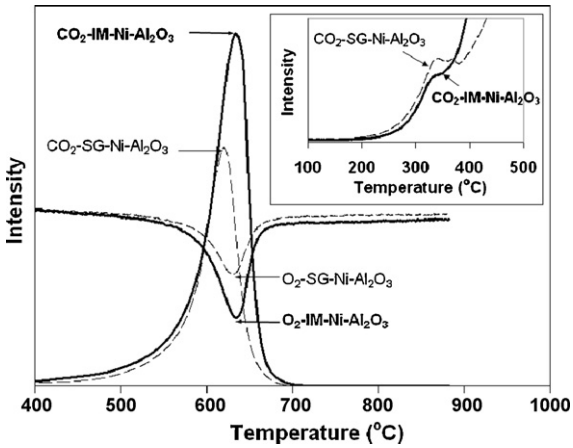

Fig. 7. Temperature-programmed oxidation profiles of carbon deposited on post-reaction Ni–Al_2O_3 catalysts.

3.5. Steam reforming of propane over reduced Ni–Al_2O_3 catalysts

Reduced (600 °C) 20% Ni–Al_2O_3 catalysts prepared by sol–gel and impregnation methods were evaluated with regard to activity, product distribution and stability in propane steam reforming at 500 °C. The feed composition used in the experiments was $C_3H_8/H_2O/N_2 = 1/4/80$. The products are H_2 and C-containing species (CO, CO_2, and CH_4 with CO_2 being the main one) from propane steam reforming.

Fig. 4 presents the C_3H_8 conversion over the catalysts prepared by the two different techniques. The reaction conditions are chosen so that complete conversion is not reached in these experiments. As seen in Fig. 4, the conversion levels over the two catalysts are comparable initially. However, the IM-Ni–Al_2O_3 catalyst shows a much faster decline in activity compared to the SG-Ni–Al_2O_3 catalyst. By

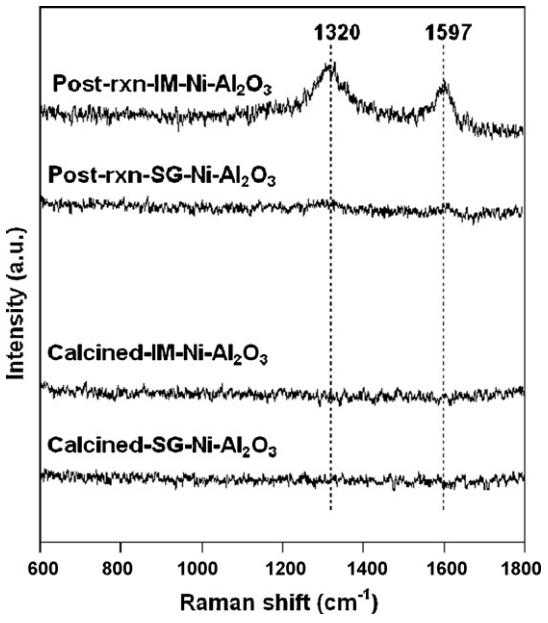

Fig. 8. Raman spectra of calcined and post-reaction Ni–Al_2O_3 catalysts.

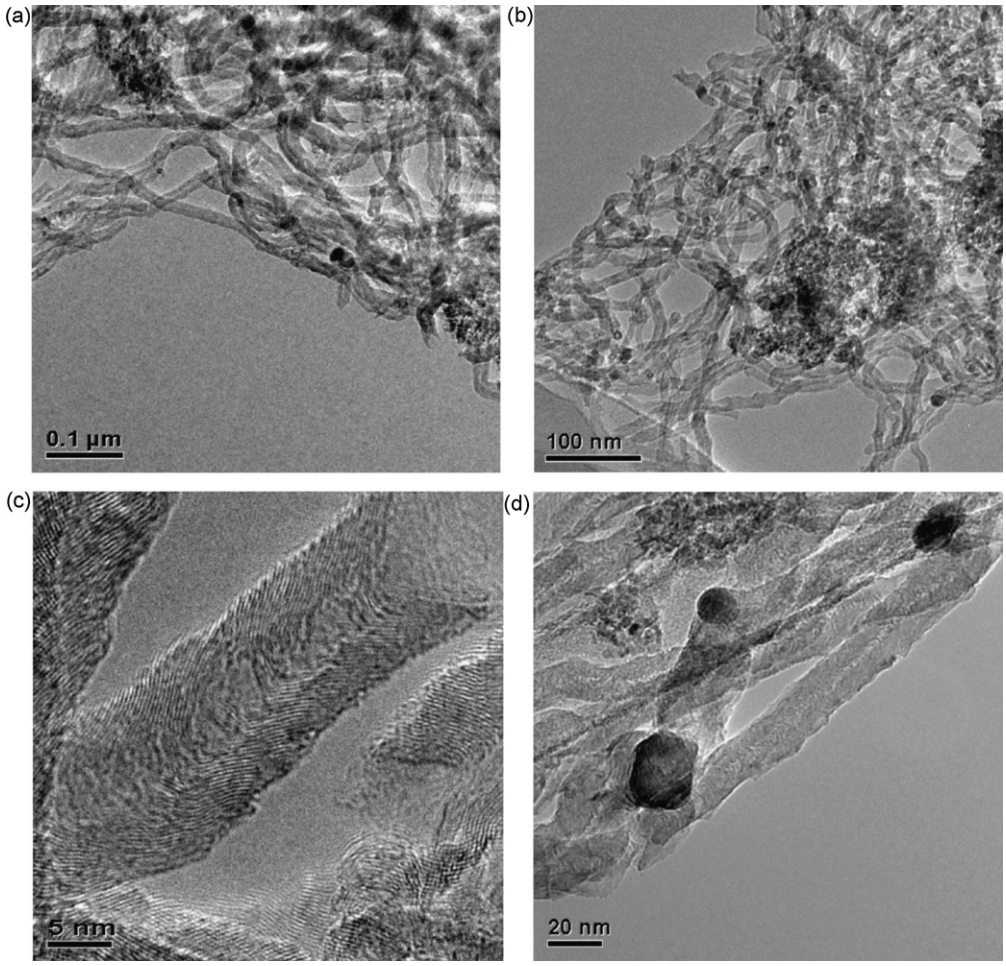

Fig. 9. Post-reaction TEM images of IM-Ni–Al_2O_3 catalysts.

the 19th hour on-stream, the IM catalyst is seen to lose more than half of its activity. The stability difference presented in Fig. 4 could be associated with the Ni cluster size. There has been discussion in the literature about the relationship between metallic Ni size and catalyst stability [2,14,16,28,42,43]. Larger Ni particle size catalyzes the coke formation reaction, which is detrimental for catalyst stability. Also, as shown by the *in situ* X-ray diffraction, IM-Ni–Al_2O_3 catalyst is more likely to lead to Ni particle size growth through sintering. TEM images to be discussed later provide visual evidence of Ni sintering taking place during reaction. It is clear that catalyst preparation plays an important role in determining Ni dispersion and particle size, metal–support interaction and morphology. Similar observations have been reported earlier for Ni-based catalytic systems [32,33,35].

The hydrogen yields and the selectivities of carbon-containing products (CO, CO_2, CH_4) are presented in Figs. 5 and 6, respectively. It should be noted that under these conditions, thermodynamic equilibrium would lead to complete propane conversion and a H_2 yield of 62%. The equilibrium selectivities for CO_2, CO and CH_4 would be 43%, 25% and 32%, respectively. So, it is clear that the product distributions in our experiments are not dictated by thermodynamic equilibrium. Although the propane conversion levels are comparable at the beginning of the run, the H_2 yields show a major difference between the two catalysts right from the beginning, with the SG catalyst giving a much higher hydrogen yield. Another interesting feature seen in Fig. 5 is the fact that hydrogen yields remain fairly constant in spite of the decline in conversion seen over the IM catalyst. When the carbon-containing product selectivities are examined, there appear to be important differences as well. Over the IM-Ni–Al_2O_3 catalyst, CH_4 is the main C-containing product at the beginning of the run. As the activity of the catalyst declines, the CH_4 selectivity also decreases, with accompanying increases in CO_2 and CO selectivities. The opposing trends between the COx selectivities and CH_4 selectivity can partly explain why H_2 yield remains constant in spite of the decreasing propane conversions.

The selectivities over the SG-Ni–Al_2O_3 catalyst, are much more constant compared to their counter-parts observed over the IM catalyst. The major C-containing product is CO_2, followed by CH_4 and CO. There is a slight decrease in CO_2 selectivity accompanied by a slight increase in CH_4 selectivity. These changes correspond to the slight decline in activity after the 14th hour on stream over this catalyst.

3.6. Coke deposition characterization on post-reaction catalysts

In this section, temperature-programmed oxidation and Raman spectroscopy were used to characterize the propane steam reforming post-reaction catalysts. TPO experiments were performed with 5% O_2/He (40 cm^3 (STP)/min) at a ramp rate of 10 °C/min from room temperature to 900 °C. Two peaks were observed from the TPO profile (Fig. 7). A low temperature peak around 350 °C is likely caused by combustion of highly reactive monoatomic carbon species deposited on Ni surfaces (Type I). Another peak of

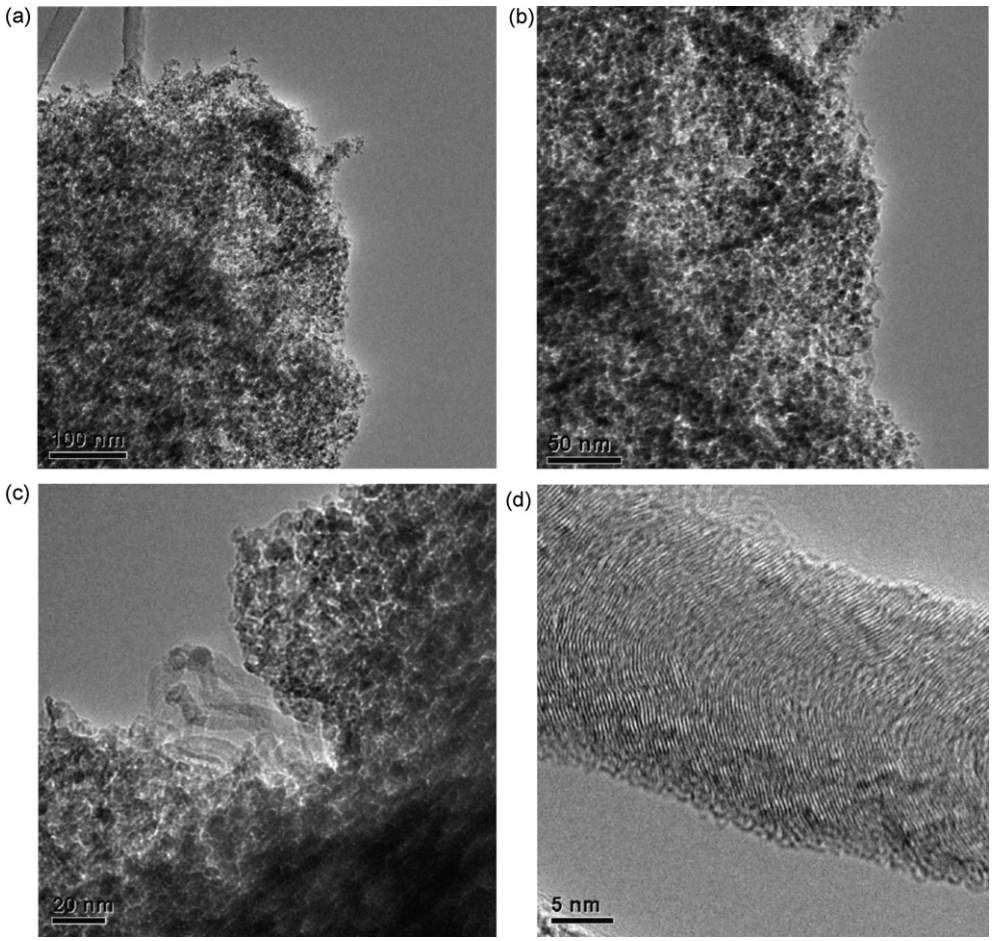

Fig. 10. Post-reaction TEM images of SG-Ni–Al_2O_3 catalysts.

much higher intensity around 630 °C can be assigned to filamentous carbon (Type II), which is typically stable and oxidized at higher temperatures [27,44,45]. Because of large intensity scale differences for these two carbon oxidation peaks, the low temperature oxidation peak was plotted as an inset in Fig. 7. It is shown that sample preparation leads to differences in this low temperature feature. For SG catalysts, there is a plateau between 330 °C and 380 °C resulting from Type I carbon oxidation before the major Type II carbon combustion takes off. This peak for IM catalyst has lower intensity and it quickly evolves into Type II carbon combustion stage. Although the trends of CO_2 evolution and O_2 consumption are similar for the two post-reaction catalysts, the amount of CO_2 produced and O_2 consumed during the oxidation of carbon deposits on 20% Ni–Al_2O_3 catalysts are significantly different. A much larger amount of carbon is deposited on Ni–Al_2O_3 catalysts prepared by the impregnation method during steam reforming of propane. The ratio of CO_2 produced for IM/SG catalysts is about 1.5 as calculated by integrating the peak area under the $m/z = 44$ evolution curve.

Fig. 8 shows the Raman spectra of Ni–Al_2O_3 catalysts in fresh and spent form. Two distinctive bands are observed for post-reaction IM-Ni–Al_2O_3 catalyst, at 1320 cm^{-1} and 1597 cm^{-1}. However, on SG-Ni–Al_2O_3 catalyst, they are very weak and broad. The 1200–1700 cm^{-1} Raman spectra region is widely used to study disorder in carbon structures, with two characteristic bands: D bands around 1339–1345 cm^{-1} and G band around 1592–1597 cm^{-1} [46]. The peak broadening for sol–gel sample indicates a very poorly graphitized structure. The more visible peak for impregnated catalysts suggests that a certain ordering of the carbonaceous deposit is developing under steam reforming reaction conditions used in this study.

3.7. TEM characterization of post-reaction samples

TEM images acquired of the post-reaction samples show major differences in the way carbon was deposited on these catalysts. Figs. 9 and 10 show the images of post-reaction IM-Ni–Al_2O_3 and SG-Ni–Al_2O_3 catalysts, respectively. A comparison of the images point to major differences in the way carbon is deposited over these two catalysts. Over the impregnated post-reaction sample, carbon deposition is exclusively in the form of long filaments, some being as long as 500 nm or more. Some fibers have hollow cores with Ni particles at the tip. Although most of the fibers have a diameter of about 15 nm, there are some with much larger diameters. Some of the particles found at the tip of the fibers are no longer spherical, but elongated along the axis of the fibers, some of them exhibiting dimensions over 35 nm in one direction (Fig. 9(d)). Because the size of Ni particles determines the carbon filament diameter [27,44], the carbon filament diameter distribution is suggestive of a non-uniform distribution of Ni particle sizes. There are two possible reasons that could lead to a non-uniform size distribution. The impregnation method used for the preparation may generate different dimensions of Ni ensembles. Additionally, Ni particles on impregnated catalysts may tend to aggregate and form larger particles under reduction and reaction conditions. The presence of large Ni particles accelerates the coke formation reaction, as evidenced by the heavily carbon-covered catalysts from the TEM images.

For the sol–gel post-reaction sample, fiber growth is markedly suppressed (Fig. 10). Although there are filaments, they are significantly shorter and thinner. Most of the particles still seem to be on the surface and no large Ni ensembles are seen. In fact most of the particles seem to be less than 10 nm. This is in agreement with the high Ni dispersion and small particle size in sol–gel preparation. It also suggests that there is no sintering of Ni during reduction or reaction as seen over the impregnated sample. Some of the fibers appear to be solid as seen in Fig. 10(d). Most fibers are well crystallized, but there is amorphous carbon as well, suggesting that the weak ordering revealed by the Raman spectroscopy might be because of the small percentage of graphite carbon fibers in the post-reaction sample.

Combining the surface and structural examination on Ni–Al_2O_3 catalysts prepared by the sol–gel and impregnation techniques, reaction tests, post-reaction sample characterization and earlier studies by our group [26,27], it appears that the preparation technique leads to significant differences in the way coking takes place on the surface. The fiber growth observed over the impregnated sample is typical of a mechanism that involves dissolution and diffusion of carbon into the metal, which results in lifting of the metal particles from the support surface as fibers grow [47]. Carbon formation mechanisms, the effect of diffusion paths and surface morphologies over supported metal catalysts have been discussed extensively in the literature, with representative discussions in [48–50].

During the steam reforming process, propane initially cracks into CH_x fragments and dissociatively adsorbs on the surface of metallic Ni particles. Subsequently, the adsorbed CH_x fragments react with oxygen-containing surface species to produce CO and H_2. The CH_x fragments could further decompose to carbon and dissolve into Ni particles. With increased carbon formation on the Ni surface, the concentration gradient induces more carbon to diffuse through the Ni particle towards the Ni–support interface, where the carbon interacts with the Al_2O_3 surface and accumulates, leading to carbon filament growth. The growth of carbon filament could break the attachment between metal and the support and lift the metal particle up. The carbon fiber growth results in a significant expansion of the catalyst bed, severe operation problems and substantial activity loss.

For catalysts prepared by impregnation method, Ni particles weakly attach to the support, which makes it easier for the particles to detach from Al_2O_3 surfaces. For catalysts prepared by sol–gel technique, Ni particles bond strongly with the support and part of the particles may be anchored into the Al_2O_3 matrix. The chemical bonding between Ni particles and the support prevents Ni particles from leaving the support, thus retarding the formation of carbon filament. Part of the coking on the sol–gel sample may also be through an "extrusion" process where carbon, instead of dissolving and diffusing into the metal particle, "extrudes" over it, thus leaving the metal particle intact on the surface. The solid filaments seen over SG samples with a "stacked-platelet structure" with no hollow core may be the result of such a process. Some of the "extruded" carbon can also be in amorphous form.

4. Summary

Compared with conventional impregnation methods, one pot sol–gel preparation yields Ni–Al_2O_3 catalysts with highly dispersed Ni particles on the surface and a strong metal–support interaction. Ni crystallite size over the sol–gel sample is relatively small and thermally stable under reaction conditions, which suppresses the carbon filament formation and filament growth. The chemical binding between metal and support on sol–gel catalysts minimizes Ni sintering at high temperatures and suppresses carbon dissolution and diffusion into Ni particles, protecting them from lifting up from the surface during carbon filament growth. Therefore, a much more stable catalytic performance is achieved with sol–gel catalytic system.

Acknowledgments

The financial support provided by Honda Research Institute, USA Inc., the National Science Foundation (NSFDMR grant # 0114098), the Ohio Department of Development (342-0561 and OCRC4-06-3-C3.31) is gratefully acknowledged.

References

[1] D.E. Ridler, M.V. Twigg, Catalyst Handbook, 2nd ed., ICI, Wolf Publishing Ltd., London, 1989, p. 225.
[2] F. Pompeo, N.N. Nichio, M.M.V.M. Souza, D.V. Cesar, O.A. Ferretti, M. Schmal, Appl. Catal. A: Gen. 316 (2007) 175.
[3] V. Modafferi, G. Panzera, V. Baglio, F. Frusteri, P.L. Antonucci, Appl. Catal. A: Gen. 334 (2008) 1.
[4] K.M. Hardiman, T.T. Ying, A.A. Adesina, E.M. Kennedy, B.Z. Dlugogorski, Chem. Eng. J. 102 (2004) 119.
[5] Q. Ming, T. Healey, L. Allen, P. Irving, Catal. Today 77 (2002) 51.
[6] J.R. Rostrup-Nielsen, I. Alstrup, Catal. Today 53 (1999) 311.
[7] M.C.J. Bradford, M.A. Vannice, Appl. Catal. A: Gen. 142 (1996) 73.
[8] J.T. Richardson, S.A. Paripatyadar, Appl. Catal. A: Gen. 61 (1990) 293.
[9] A. Igarashi, T. Ohtaka, S. Motoki, Catal. Lett. 13 (1991) 189.
[10] J.R. Rostrup-Nielsen, J.H. Hansen, J. Catal. 144 (1993) 38.
[11] D.L. Qin, J. Catal. Today 21 (1994) 551.
[12] R. Craciun, B. Shereck, R.J. Gorte, Catal. Lett. 51 (1998) 149.
[13] X. Wang, R.J. Gorte, Catal. Lett. 73 (2001) 15.
[14] J.H. Edwards, A.M. Maitra, Fuel Process. Technol. 42 (1995) 269.
[15] Y.-G. Chen, K. Tomishige, K. Yokoyama, K. Fujimoto, J. Catal. 184 (1999) 479.
[16] L. Pelletier, D.D.S. Liu, Appl. Catal. A: Gen. 317 (2007) 293.
[17] J.R. Rostrup-Nielsen, Catalytic Steam Reforming, in: J.R. Anderson, M. Boudart (Eds.), Catalysis: Science and Technology, 5, Springer Verlag, New York, 1984, p. 3.
[18] T. Borowiecki, A. Golebiowski, Catal. Lett. 25 (1994) 309.
[19] T. Borowiecki, A. Golebiowski, B. Stasinska, Appl. Catal. A: Gen. 153 (1997) 141.
[20] B. Stasinska, A. Golebiowski, T. Borowiecki, in: B. Delmon, G.F. Froment (Eds.), Catalyst Deactivation, Elsevier, Amsterdam, 1999, p. 431.
[21] T. Borowiecki, A. Machocki, in: B. Delmon, G.F. Froment (Eds.), Catalyst Deactivation, Elsevier, Amsterdam, 1999, p. 435.
[22] T. Borowiecki, G. Giecko, M. Panczyk, Appl. Catal. A: Gen. 230 (2002) 85.
[23] Q. Zhuang, Y. Qin, L. Chang, Appl. Catal. 70 (1991) 1.
[24] S. Wang, G.Q. Lu, Appl. Catal. B: Environ. 19 (1998) 267.
[25] R.M. Sambrook, J.R.H. Ross, US Patent 4 469 815 (1984).
[26] S. Natesakhawat, O. Oktar, U.S. Ozkan, J. Mol. Catal. A: Chem. 241 (2005) 133.
[27] S. Natesakhawat, R.B. Watson, X. Wang, U.S. Ozkan, J. Catal. 234 (2005) 496.
[28] A. Slagtern, Y. Schuurman, C. Leclercq, X. Verykios, C. Mirodatosy, J. Catal. 172 (1997) 118.
[29] Z. Hou, T. Yashima, Appl. Catal. A: Gen. 261 (2004) 205.
[30] J.-H. Kim, D.-J. Suh, T.-J. Park, K.-L. Kim, Appl. Catal. A: Gen. 197 (2000) 191.
[31] H. Hayashi, S. Murata, T. Tago, M. Kishida, K. Wakabayashi, Chem. Lett. 30 (2001) 34.
[32] B.S. Liu, C.T. Au, Appl. Catal. A: Gen. 244 (2003) 181.
[33] H.Y. Wang, E. Ruckenstein, Appl. Catal. A: Gen. 209 (2001) 207.
[34] B. Jongsomjit, J. Panpranot, J.G. Goodwin Jr., J. Catal. 215 (2003) 66.
[35] Y. Chen, J. Ren, Catal. Lett. 29 (1994) 39.
[36] U.S. Ozkan, Y. Cai, M.W. Kumthekar, L. Zhang, J. Catal. 142 (1993) 182.
[37] X. Wang, U.S. Ozkan, J. Phys. Chem. B 109 (2005) 1882.
[38] M.L. Jacono, M. Schiavello, A. Cimino, J. Phys. Chem. 75 (1971) 1044.
[39] K.T. Ng, D.M. Hercules, J. Phys. Chem. 80 (1976) 2094.
[40] R.D. Gonzalez, T. Lopez, R. Gómez, Catal. Today 35 (1997) 293.
[41] M.H. Youn, J.G. Seo, P. Kim, I.K. Song, J. Mol. Catal. A: Chem. 261 (2007) 276.
[42] V.R. Choudhary, A.S. Mamman, Appl. Energ. 66 (2000) 161.
[43] J.S. Lisboa, D.C.R.M. Santos, F.B. Passos, F.B. Noronha, Catal. Today 101 (2005) 15.
[44] P. Wang, E. Tanabe, K. Itob, J. Jia, H. Morioka, T. Shishido, K. Takehira, Appl. Catal. A: Gen. 231 (2002) 35.
[45] S. Wang, G.Q. Lu, Ind. Eng. Chem. Res. 38 (1999) 2615.
[46] J. Llorca, N. Homs, J. Sales, P. Ramírez de la Piscina, J. Catal. 209 (2002) 306.
[47] N.M. Rodriguez, J. Mater. Res. 8 (1993) 3233.
[48] J.-W. Snoeck, G.F. Froment, M. Fowlesz, J. Catal. 169 (1997) 240.
[49] J.-W. Snoeck, G.F. Froment, M. Fowlesy, J. Catal. 169 (1997) 250.
[50] R.T.K. Baker, M.A. Barber, P.S. Harris, F.S. Feates, R.J. Waite, J. Catal. 26 (1972) 51.